Sensors & Actuators: B. Chemical 305 (2020) 127550

Contents lists available at ScienceDirect

Sensors and Actuators B: Chemical

journal homepage: www.elsevier.com/locate/snb

M-Nx (M = Fe, Co, Ni, Cu) doped graphitic nanocages with High specific surface Area for non-enzymatic electrochemical detection of H_2O_2

Zhao Min Sheng*[,1], Zu Zhong Gan, Huan Huang, Rui Liang Niu, Zhi Wei Han, Run Ping Jia*

School of Materials Science and Engineering, Shanghai Institute of Technology, Shanghai 201418, China

ARTICLE INFO

Keywords:
Biosensor
Template-approach
High specific surface area
Efficient catalysis
Floating catalytic pyrolysis

ABSTRACT

N-doped porous-walled graphitic nanocages (NGCs) with high specific surface area have been successfully doped by metallic ions (M^{2+} = Fe^{2+}, Co^{2+}, Ni^{2+} or Cu^{2+}) for efficiently detecting H_2O_2. To increase surface area, NGCs were prepared by partially removing N-doped template inserted in their graphitic layers to sharply create nanopores in graphitic shells of nanocages, which were approached from removing ferrous cores of core-shell precursor (Fe_3C@NDC) synthesized from short-time floating catalytic pyrolysis. With high specific surface area (920 $m^2 g^{-1}$), mesopore volume (1.6 $cm^3 g^{-1}$) and good graphitization, the synergistic effects of metallic ions and N-doped structure, which improves their dispersion and increases active sites, plays a very important role in detection of H_2O_2. Fe-N coordination much easier forms in the condition of our experiment than Co-N, Ni-N and Cu-N, which might lead to better electrochemical performance of Fe-Nx doped graphitic nanocages (Fe-NGCs), including wider linear range (0.001 − 5 mM), lower LOD (0.53 μM), higher sensitivity (184.4 μA mM^{-1} cm^{-2}), selectivity and stability. Such results demonstrate Fe-NGCs nanocomposite is a promising candidate for the detection of H_2O_2 in practical application.

1. Introduction

Hydrogen peroxide (H_2O_2) is produced as metabolic byproducts or intermediates in several highly selective oxidases of cells growth [1,2]. Thus, some diseases including cancer, diabetes, heart diseases and neurodegeneration etc, can be detected by the concentration of H_2O_2 in the body [3–5]. Additionally, H_2O_2 is widely used as oxidizer, disinfectant or bleach in food, environmental analysis, chemical and pharmaceutical industry etc [6,7], leading to hydrogen peroxide plays an important role in the development of sensors, including titration [8,9], spectrometry [10,11], chromatography [12,13], chemiluminescence [14,15], electrochemistry [16–18] and so on. Compared to the above methods, the electrochemical method is promising in detection of H_2O_2 with inherent advantages, including low cost, easy operation, fast response and portability [1,4]. The enzyme-based biosensors are unique in sensitivity and selectivity, while complex enzyme immobilization, specific operating conditions, inactivation in a non-fixed environment and high cost limit their practical application [2,18]. In order to break through these restrictions, some non-enzymatic sensors modified by noble metals, such as Au [19], Ag [20], Pt [21] and Pd [22], have achieved higher sensitivity, wider detection concentration range and lower detection limit [11]. However, the industrial production of such prepared sensors is limited by low natural abundance of noble metals.

In recent years, non-noble metal nanomaterials have a good prospect in electrochemical detection of H_2O_2 by amperometry, cyclic voltammetry (CV) and differential pulse voltammetry (DPV) [23–27]. DPV technique is suitable to detect H_2O_2 in its lower concentration solution [23], while the advantage of the amperometry is its readable data and available in commercial application [24–30]. Additionally, the transition metal compounds (e.g. Fe, Co, Ni, etc.) have attracted attention due to their unique structural properties and low cost [24], leading to their sharp development: well-crystallized Fe_3O_4 nanoparticles were loaded on reduced graphene oxide [6]; α-Fe_2O_3 nanoparticles were deposited on the surface of NiO nanosheets [24]; Fe_3C nanoparticles were loaded on functionalized 3D N-doped carbon structures [28]. Furthermore, Prussian blue (PB), protein and polymer were introduced onto ferrous compounds to improve performance of detecting H_2O_2 [29–31]. On the other hand, carbon nanomaterials such as graphene, carbon fiber and carbon nanotubes are widely used as carriers for metallic nanostructure because of their unique features such as fast electron transfer, excellent biocompatibility, relatively wide potential window and feasibility for surface functionalization [24,24,25,26,27]. To get over agglomeration and low dispersion, metallic or carbon nanomaterials are usually modified by surfactants,

* Corresponding authors.
E-mail addresses: zmsheng@sit.edu.cn (Z.M. Sheng), jiarp@sit.edu.cn (R.P. Jia).
[1] These authors contributed equally to this work.

https://doi.org/10.1016/j.snb.2019.127550
Received 20 October 2019; Received in revised form 24 November 2019; Accepted 6 December 2019
Available online 09 December 2019
0925-4005/

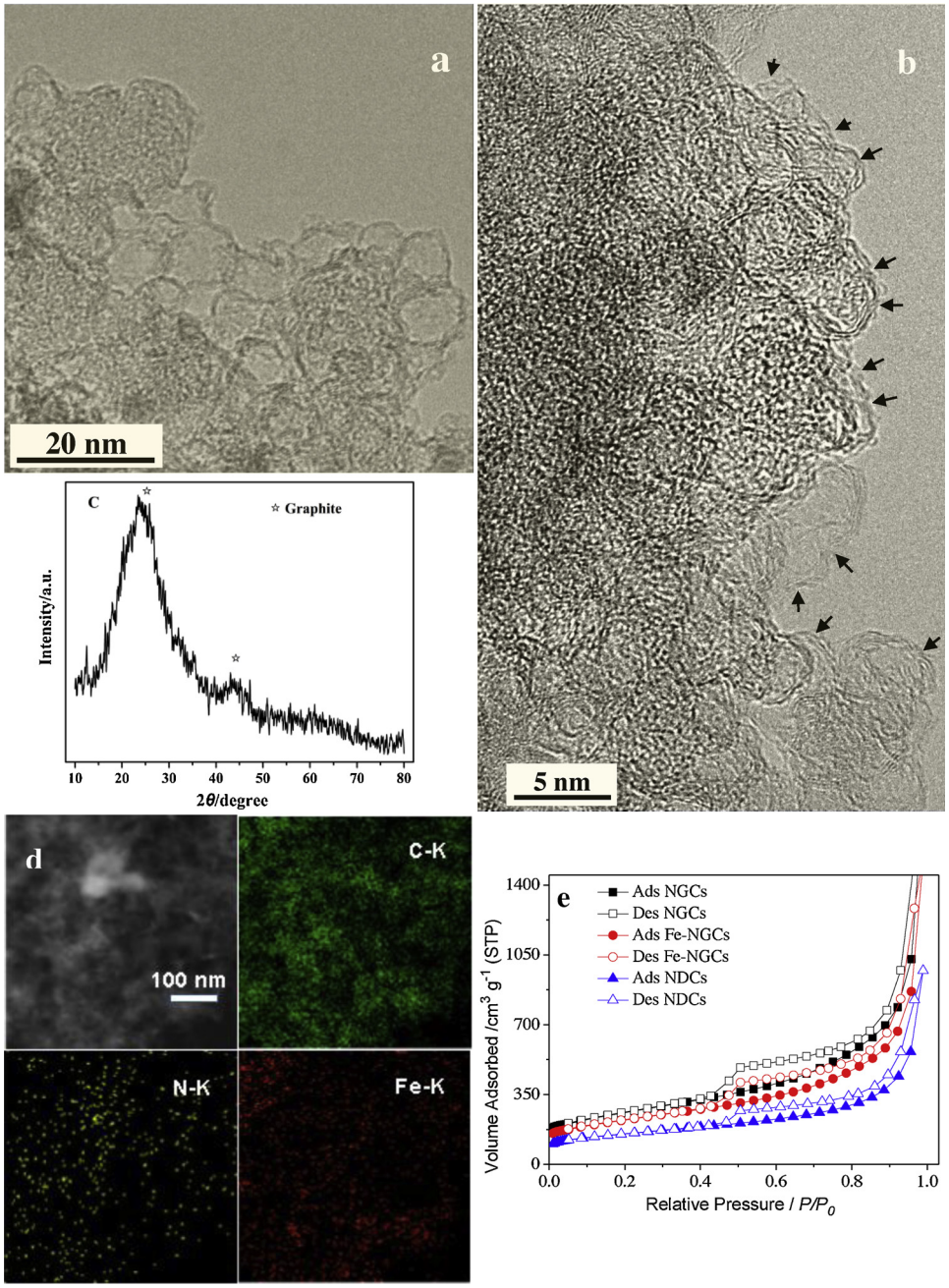

Fig. 1. TEM (a) and HRTEM (b) images of Fe-NGCs, (c) XRD pattern of Fe-NGCs, (d) Elemental mapping images of C, N, Fe of Fe-NGCs, (e) N_2 adsorption/desorption isotherms of the NDCs, pore created NGCs and Fe-NGCs.

which are difficult to be removed and inhibit catalytic activity [19]. Another strategy has been developed that reduced graphene oxide supports transition metal sulfide to provide more active sites and good electrical conductivity [1,12], which is limited by their low specific surface area ($< 550\ m^2\ g^{-1}$) [5,7,17]. To increase active sites, polymer-based precursors have been employed to modify the metallic nanostructure, and a catalyst with high activity is obtained after its carbonization. Since high carbonization temperature usually trades off property of surface area and surface reactivity [32–34], their low carbonization temperature ($\leq 800\ ^\circ C$) [2,22] might influence their graphitization, conductivity and resistance to corrosion [6,16,24]. Some graphitic substrates were synthesized by floating catalytic pyrolysis. Due to the short synthetic time and controllable pyrolytic temperature, the diameters of such prepared substrates became smaller [33–35].

Herein, N-doped porous-walled graphitic nanocages (NGCs) with high specific surface area have been successfully doped by metallic ions (M^{2+} = Fe^{2+}, Co^{2+}, Ni^{2+} or Cu^{2+}) for efficiently detecting H_2O_2. To increase surface area, NGCs were prepared by partially removing N-doped template inserted in their graphitic layers to sharply create nanopores in graphitic shells of nanocages, which were approached from removing ferrous cores of core-shell precursor (Fe_3C@NDC) synthesized from short-time floating catalytic pyrolysis. High specific surface area of such prepared NGCs is useful to improve dispersion of metallic ions and increase active sites leading to efficient electrocatalysis of NGC-modified glassy carbon electrodes (GCEs). As far as we know, there is no report on Fe and N co-doped graphitic materials with so high specific surface area for detecting H_2O_2 until now.

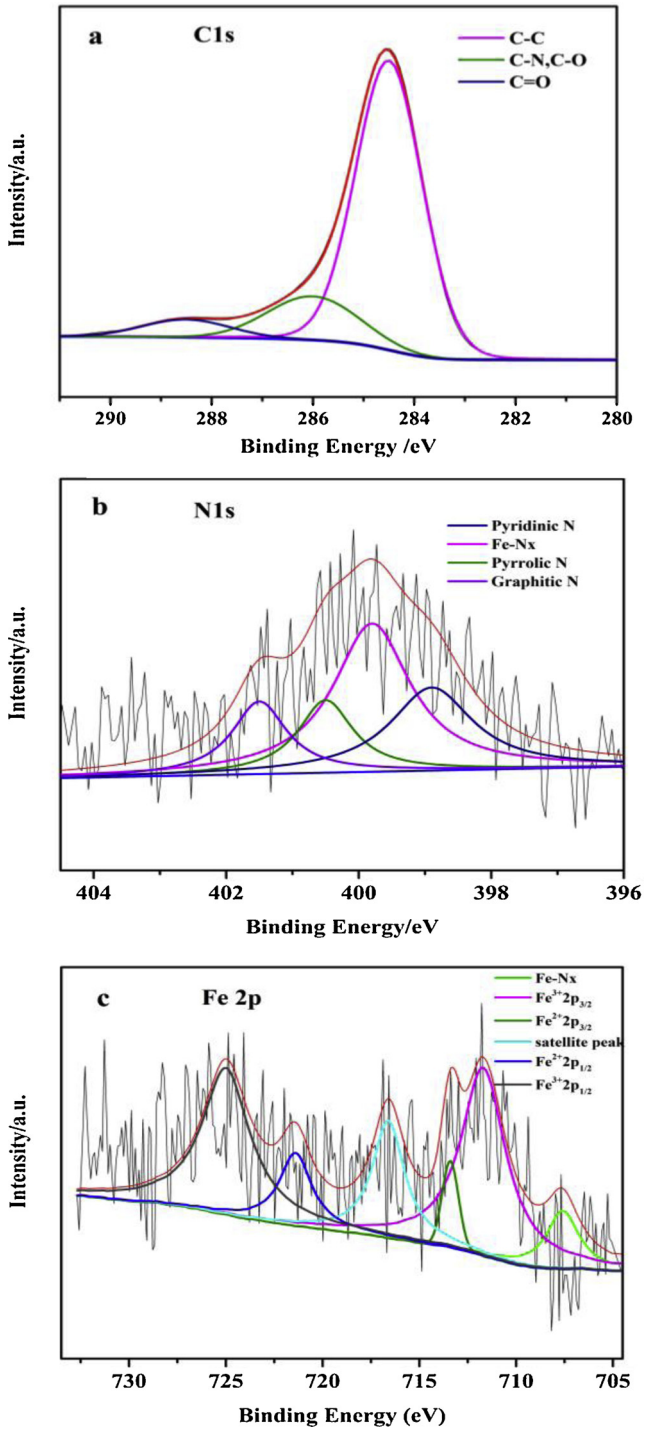

Fig. 2. XPS spectra of the Fe-NGCs. (a) C1s, (b) N1s and (c) Fe2p.

2. Experimental section

2.1. Synthesis of M-NGCs

The porous N-doped graphitic nanocages (NGCs) were prepared by removing iron core from core-shell precursor (Fe_3C@NDC) which were synthesized through floating catalytic pyrolysis of gas mixture in the quartz tube at 900 °C. The gas mixture including acetylene (carbon sources, 10 ml min^{-1}), NH_3 (nitrogen sources, 100 ml min^{-1}), N_2 (carrier gas, 80 l h^{-1}) and carried iron pentacarbonyl (catalysts sources), flew through high temperature area of furnace in a few seconds, and then Fe_3C@NGS could be collected at the other end of the quartz tube. In order to remove iron core and iron ions, the Fe_3C@NDC were pickled with stirring in mixed acid (HCl:HNO_3 = 10:1) at 70 °C for 8 h, and then were filtered repeatedly after stayed still overnight. After freeze-drying to remove water, the NDCs were annealed in vacuum at 300 °C for 1 h to partially eliminate N-doped template to get the pore created (PC) NGCs. Finally, the M-NGCs were prepared by adding the NGCs with 40 mg into 150 ml 0.1 M $FeCl_3$, $CuSO_4$, $Co(NO_3)_2$ or Ni $(NO_3)_2$ solution with ultrasonic oscillation for 12 h, and then the M-NGCs were filtrated and dried.

2.2. Characterizations

The microcosmic structure and morphology of prepared materials were characterized by high resolution transmission electron microscopy (HRTEM: JEOL, JEM-2100 F) and corresponding energy dispersive spectroscopy (EDS) mapping. The crystallographic information was investigated by X-ray diffraction (XRD: Bruker D8 Advance, Bruker AXS, Germany). The surface composition was analyzed through X-ray photoelectron spectroscopy (XPS: thermos ESCALAB 250Xi). The surface area and pore structure were characterized by nitrogen adsorption/desorption measurement (ASAP 2020, Micromeritics).

2.3. Electrochemical measurements

All electrochemical measurements were tested by using a three-electrode system at room temperature with an electrochemical workstation (CHI760E, CH Instruments, USA). The working electrode was prepared with coating catalysts slurry onto GCEs with 3 mm diameter, and catalyst slurry was made ready to disperse 1 mg catalysts powder in a mixture of ethanol (0.95 ml) and 5% Nafion solution (0.05 ml) with sonication treatment for 1 h. For fair comparison, all catalysts were loaded on the GCEs with the same loading amount (1.4 μg mm^{-2}). Moreover, a saturated calomel electrode (SCE) and a platinum wire were used as the reference electrode and the counter electrode, respectively. The CV and the chronoamperometry (i–t) were conducted in 0.1 M phosphate buffer (PB: pH = 7) solution. The electrochemical impedance spectroscopy (EIS) were recorded with a frequency range of 1-10^6 Hz and the DC bias and amplitude voltages were set at 0.26 V and 0.005 V, respectively.

3. Results and discussion

3.1. Characterization of M-NGCs

The nanostructures and crystal structures of Fe-NGCs are probed by HRTEM. According to the result (Fig. S1a) shown in Supplementary Information (SI), the core-shell precursors (Fe_3C@NDC) prepared by thermal pyrolysis at 900 °C are 4 ~ 15 nm Fe_3C (cementite) nanoparticles coated with N-doped graphitic shells. The Fe_3C cores wrapped by the carbon layer can be basically removed from Fe_3C@NDC by acid treatment (Fig. S1b). After acid and annealing treatment, lots of nanopores are formed in graphitic shells by partially removing N-doped template and most thin graphitic shells are completely preserved to NGCs in Fig. S1b. Simultaneously, the unique nanoporous graphitic structure of NGCs is inherited by Fe-NGCs after Fe ions are attached to N-doped structure (Fig. 1a and b). The diffraction peak of Fe-NGCs shown in Fig. 1c and its HRTEM image shown in Fig. 1b indicate that the Fe-NGCs possesses good graphitization with ~1 nm moderate graphitic shell. Furthermore, the elemental mapping shows Fe-NGCs consist of C, N and Fe, and they are uniformly distributed within nanocages (Fig. 1d). Thus, such results confirm the Fe-NGCs with nanoporous graphitic structure have been prepared.

To further investigate changes of nanoporous structures after pickling and annealing treatment, the samples are measured through N_2 adsorption/desorption isotherms (Fig. 1e). The specific surface area (S_{BET}) and mesopore volume for the NDCs are 630 $m^2 g^{-1}$ and

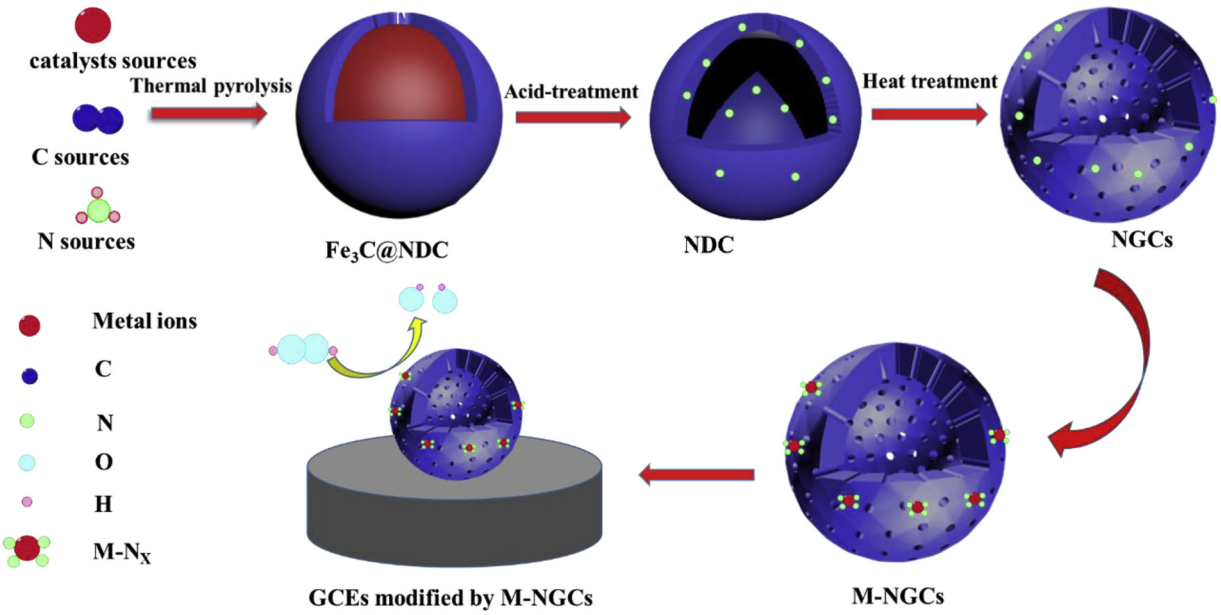

Fig. 3. Scheme of synthetic pathway of M-NGCs nanocomposite which modifies GCEs to detection of H_2O_2.

0.87 $cm^3 g^{-1}$, respectively. In comparison, specific surface area (S_{BET}) (NGCs vs. Fe-NGCs = 980 $m^2 g^{-1}$: 920 $m^2 g^{-1}$) and mesopore volume (NGCs vs. Fe-NGCs = 1.7 $cm^3 g^{-1}$: 1.6 $cm^3 g^{-1}$) are rapidly increased after pickling and annealing treatment [35,36], and Fe-NGCs has basically no change in nanoporous structures to NGCs after loading iron ion. Thus, Fe-NGCs with high specific surface area and nanoporous structure are expected to provide more accessible active sites and easier diffusion. During acid-treating Fe_3C@NDC, both N-doped structure and C atoms were partially being oxidized, according to carboxyl groups (2365 cm^{-1}) and nitro-groups (1387 cm^{-1}) sharply increased in the FTIR spectra (Fig. S2a) of NDCs (Fe_3C of Fe_3C@NDC was removed by acid treatment). As N atoms were substitutionally doped in the graphitic layers of the NDC, N-doped structure was oxidized into nitro-group leading to N—C bonds breaking. Thus, C atoms from broken N—C bonds were easily oxidized into carboxyl groups in the acid-treatment. The N and O contents of the NDCs were 3 wt.% and 12 wt.%, respectively. After annealing in vacuum, the N and O contents of the NDCs were reduced to 2 wt.% and 6 wt.% (Fig. S2b), respectively, indicating the carboxyl groups and nitro-groups formed from oxidization of N-doping structure were not stable and partially removed (NGCs in Fig. S2) to form nanopores in the graphitic shells.

The elemental composition and chemical state of samples are investigated by XPS. As shown in Fig. S3a, the Fe, Co Ni and Cu are loaded onto the surface of NGCs to form Fe-NGCs, Co-NGCs, Ni-NGCs and Cu-NGCs, respectively. There is basically no change in the valence state of carbon with C—C bond (284.6 eV), C—N or C—O bond (286.0 eV) and C═O bond (288.7 eV) (Fig. 2a, S3, S4, S5 and S6), indicating that doping transition metal element has little effect on the carbon structure. For N1s of Fe-NGCs (Fig. 2b), four types of doped nitrogen species are obtained by fitting with pyridinic N (398.8 eV), pyrrolic N (400.5 eV), graphitic N (401.5 eV) and Fe-N_x (399.8 eV). Simultaneously, the peak area ratio of the Fe-N_x bond is 43.5 %, occupying a dominant position in nitrogen species, which is far greater than 20.0 % Co-N and 20.8 % Ni-N and 25.0 % Cu-N (Fig. 2b, S4b, S5b and S6b), suggesting Fe-N coordination much easier forms in our condition than Co-N, Ni-N and Cu-N. According to Fe2p of Fe-NGCs (Fig. 2c), it is demonstrated that Fe^{3+} (711.7 eV for $Fe2p_{3/2}$, 725.0 eV for $Fe2p_{1/2}$), Fe^{2+} (713.4 eV for $Fe2p_{3/2}$, 721.4 eV for $Fe2p_{1/2}$), satellite peak (716.6 eV) and Fe-N_x (707.6 eV). Similar characteristics is observed in the Co2p, Ni2p and Cu2p spectra of Co-NGCs Ni-NGCs and Cu-NGCs (Fig. S4c, S5c and S6c) [1,17,37]. Both the proportion of transition metal element atomic number in the respective samples (1.1 at% Fe in Fe-NGCs, 0.93 at% Co in Co-NGCs, 0.97 at% Ni in Ni-NGCs and 3.92 at% Cu in Cu-NGCs) and the percentages of Fe, Co, Ni or Cu-N coordination sites in N elemental (43.5 % Fe-N, 20.0 % Co-N, 20.8 % Ni-N, 25.0 % Cu-N) illustrate the Fe-NGCs may provide a larger number active sites (as shown in Tab. S1) that contribute to the outstanding electrochemical sensing performance towards H_2O_2. The scheme of the pathway to synthesis of the Fe-NGCs sample has been shown in Fig. 3.

3.2. Electrochemical detection of H_2O_2 by sensors modified by Fe-NGCs

To study the electron exchange features at surface-modified electrode, GCEs modified by Fe-NGCs or Fe-NDCs were investigated by electrochemical impedance spectroscopy (EIS) in 0.1 M PB solution at a frequency range of 1-10^6 Hz. As shown in Fig. S7, the Nyquist plots of Fe-NGCs and Fe-NDCs is consisted by a semicircular part (which is corresponded to the charge transfer resistance (R_{ct})) of the redox reaction at the electrode/electrolyte interface) and the linear part (which contributes to the ion-diffusion process and its slope is proportional to ion-diffusion rate). The equivalent electrical model is simulated accurately to place in the illustration of Fig. S7. The value of R_{ct} is equal to the semicircle diameter of Nyquist plots, and they are estimated to be about 128 Ω (Fe-NGCs) and 200 Ω (Fe-NDCs) in Fig. S7. Compared with Fe-NDCs, Fe-NGCs has the lower resistance value and faster ion-diffusion rate, indicating that Fe-NGCs is provided with the higher electrochemical activity and conductivity.

To study the electrochemical behaviors of modified electrodes as a H_2O_2 sensor, the electrocatalytic activities of NGCs, Fe-NGCs, Co-NGCs and Ni-NGCs are investigated by CV in 0.1 M PB (pH = 7) solution in presence of 5 mM H_2O_2 at a scan rate of 50 mV s^{-1} within the potential range of 0.4 to -0.6 V (Fig. 4a). As shown in Fig. 4a, Fe-NGCs has the largest cathodic current in same condition, suggesting the highest catalytic activity of M-NGCs in prepared samples to H_2O_2 electrocatalysis. The reason is that many M-N_x active sites are equally distributed onto NGCs with high specific surface area. The mechanism of electrochemical detection of H_2O_2 can be proposed: H_2O_2 is reduced to OH- by trivalent iron of Fe-N_x active sites, as shown below Eqs. (1)–(3) [7].

$$\text{M-NGCs} + H_2O_2 \rightarrow \text{M-NGCs}\cdot H_2O_2 \quad (1)$$

$$\text{M-NGCs}\cdot H_2O_2 + e \rightarrow \text{M-NGCs}\cdot(OH) + OH^- \quad (2)$$

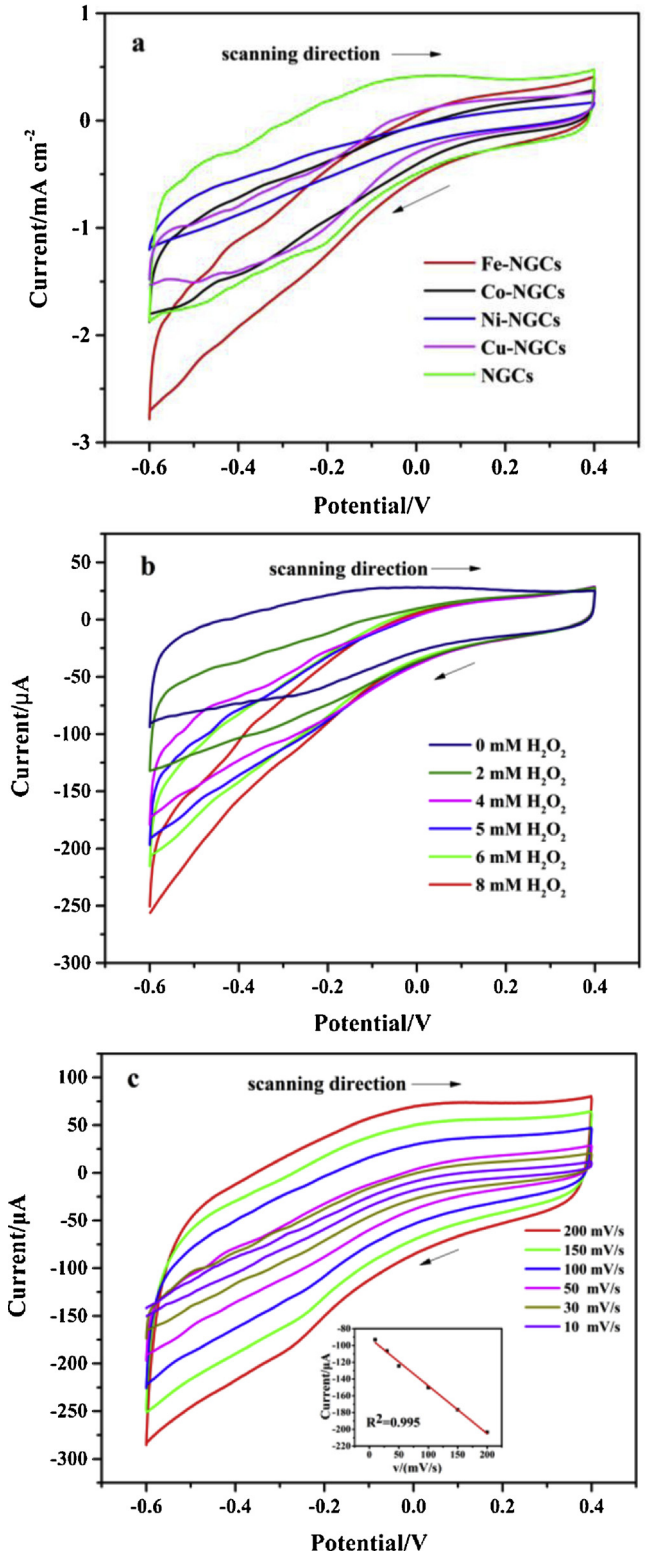

Fig. 4. (a) The CVs of the glassy carbon electrodes modified by NGCs, Fe-NGCs, Co-NGCs, Ni-NGCs or Cu-NGCs in presence of 5 mM H_2O_2 at a scan rate of 50 mV s^{-1}. (b) The CVs of the GCEs modified by Fe-NGCs in presence of different concentration of H_2O_2. (c) The CVs of the GCEs modified by Fe-NGCs in presence of 5 mM H_2O_2 at different scan rates and insert: the calibration curve of current vs. scan rate at -0.35 V (vs. SCE).

$$M\text{-}NGCs\cdot(OH) + e \rightarrow M\text{-}NGCs + OH^- \quad (3)$$

To further investigate electrochemical properties of Fe-NGCs to H_2O_2 electrocatalysis, the catalytic response of Fe-NGCs toward H_2O_2 electrocatalysis at various H_2O_2 concentrations are evaluated. The cathode current is significantly enhanced with the increasing concentration of H_2O_2 (Fig. 4b), which is a typical expression of catalytic decomposition reaction of H_2O_2. In addition, the electric transfer performance of Fe-NGCs can be measured by CV at different scan rates in presence of 5 mM H_2O_2. The cathodic current increase greatly which is proportional to the scan rate, and the calibration curve of current vs. scan rate at -0.35 V is calculated as I (μA) = -0.57 v (mV s^{-1}) - 37.87 (R^2 = 0.995) as shown in illustration of Fig. 4c. Therefore, the electrochemical kinetics for detection of H_2O_2 is controlled by diffusion and adsorption of H_2O_2 molecules, illustrating the Fe-NGCs with high specific surface area and nanoporous structure have a promising potential for detection of H_2O_2.

In order to determine the optimal detection potential for the amperometric response of the GCEs modified by Fe-NGCs to H_2O_2, the i–t curves are obtained under different potentials ranging from -0.3 ~ -0.4 V with continuous additions of H_2O_2 at interval of 50 s. As shown in Fig. S8a, the responsive current reach a maximum value at -0.35 V. Obviously, the highest current and lowest noise suggest -0.35 V can be used as the optimal detection potential. To further confirm the ability of prepared samples to electrochemical detection of H_2O_2, the amperometric responses of electrodes modified by different samples are tested with successive additions of H_2O_2 at -0.35 V (Fig. S8b). The Fe-NGCs shows much higher catalytic activity than other samples, which verifies the previous result of CV test.

The main properties (including sensitivity, linear range, and detection limit) of the GCEs modified by Fe-NGCs to detection of H_2O_2 are studied by amperometry at applied potential of -0.35 V (Fig. 5a). The illustration displays the amplified current detail of the i–t curves for low concentration of H_2O_2. It's discovered that the current responds immediately after adding H_2O_2 for about 4 s and quickly reaches steady state, indicating the GCEs modified by Fe-NGCs are provided with excellent electrocatalytic performance and fast response for H_2O_2. As shown in Fig. 5b, the liner range of the GCEs modified by Fe-NGCs response to H_2O_2 is applied in H_2O_2 concentration range from 1 μM to 5 mM, and the liner regression equation is as follows: I (μA) = -13.32C (mM)-24.41 (R^2 = 0.99). An excellent sensitivity which reach 180 μA mM^{-1} cm^2 is obtained by calculating the ratio of the slope of the liner regression equation and GC electrode area. The limit of detection (LOD) of this electrode to H_2O_2 is calculated to be 0.53 μM by the formula: LOD = 3(RSD/slope) (where RSD is the standard deviation to the average measurement of blank sample, slope is from the liner regression equation) [1,19,20].

It is noticed that excellent activity and favorable performance of Fe-NGCs for sensing H_2O_2 is ascribed to their own unique structure with high specific surface area and good graphitization: high specific surface area of NGCs with uniformly N-doping synergistically promote uniform distribution of Fe ions to form a large number of Fe-N_x active sites and their centers have positive charge to easily adsorb HO_2^- ionizing from H_2O_2, leading to efficient H_2O_2 reduction. This can be supported by the inset in Fig. 4c: the insert shows the current is proportional to the scan rate which means the electron transfer process is controlled by adsorbed species. High specific surface area of Fe-NGCs also improves the stability of such prepared sensors by preventing Fe from agglomeration. Additionally, nanoporous structure of Fe-NGCs provides with large number of channels for fast diffusion of H_2O_2 and products to shorten their diffusion route, which might achieve a fast response to detecting H_2O_2. Simultaneously, good graphitization of Fe-NGCs enhances their conductivity to achieve rapid electron transfer and makes Fe-NGCs stable in complex electrochemical environments. Finally, the peak area ratio of the Fe-N_x bond is 43.5 %, occupying a dominant position in nitrogen species, which is far greater than 20.0 % Co-N and 20.8 % Ni-N and 25.0 % Cu-N (Figs. 2b, S4b, S5b and S6b), suggesting Fe-N coordination much easier forms in the condition of our experiment than Co-N, Ni-N and Cu-N, which might lead to the highest performance of

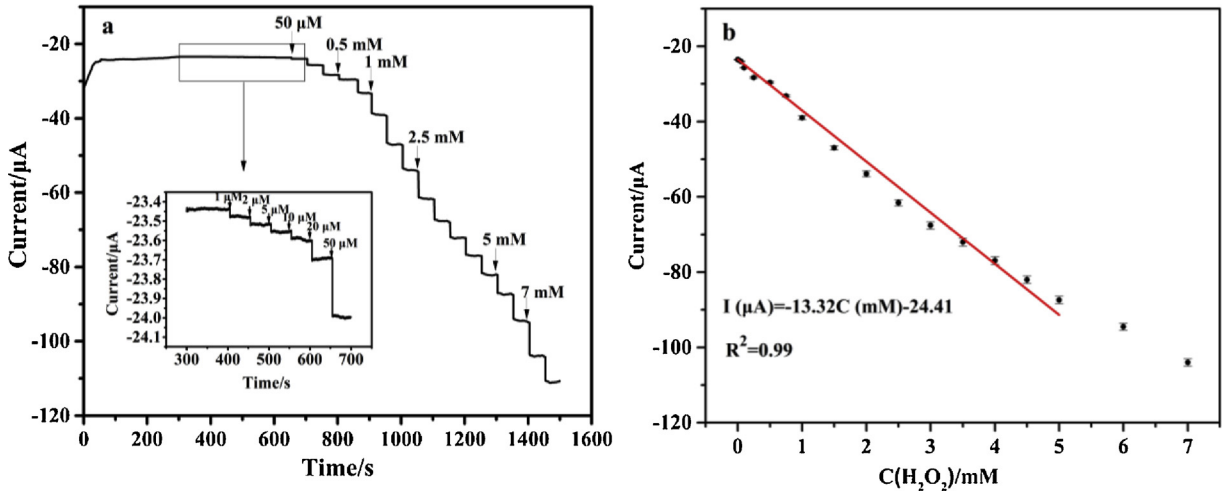

Fig. 5. (a) Amperometric response of GCEs modified by Fe-NGCs to successive additions of H_2O_2 at -0.35 V (vs. SCE) and insert: amplified portion of i–t curves for low concentration of H_2O_2. (b) The calibration curve of the GCEs modified by Fe-NGCs responding to H_2O_2.

Table 1
Comparison of the sensor modified by Fe-NGCs with reported electrochemical H_2O_2 sensors.

Modified electrodes	Medium	Linear range / mM	Detection limit / μM	Sensitivity / μA mM^{-1} cm^{-2}	Reference
$NiCo_2S_4$/rGO	0.1 M NaOH	0.025-11.25	0.19z.star;	118.5	[1]
AuNBP/MWCNTs	0.1 M PB pH = 7	0.005-47.3	1.5	170.6	[3]
$Ce_{0.9}Tb_{0.1}Oy$ crystals	0.1 M PB pH = 7.4-8	0.0001-4.2	7.7	13.0	[11]
{PEI/rGO}-Au@P_8W_{48}/ITO	0.4 M PBS pH = 7.0	–	0.31	74.6	[12]
Au-NPs/N-GQDs/GC	0.1 M PB pH = 7.4	0.00025-13.327	0.12z.star;	186.2	[19]
Ag/NCNFs	0.2 M PBS pH = 7.0	0.02-20	0.15	142.2	[5]
3D-NS-900/GCE	0.1 M PBS pH = 7.0	0.0005-14	0.18	–	[7]
AgNPs/PANI/HNT	0.1 M PBS pH = 7.0	0.0005-4.7	0.3z.star;	74.8	[20]
PVA-MWCNTs-PtNPs	0.1 M PBS pH = 7.0	0.002–3.8	0.7	122.63	[21]
NiO/α-Fe_2O_3	0.5 M PB pH = 7.0	0.5-3	50	95.6 ± 3	[24]
Fe_3C/NG	0.1 M PBS pH = 7.0	0.05-15	35	–	[28]
40 − 46 nm PB-Fe_2O_3	0.025 M PBS pH = 6.0	0.02-0.3	7	–	[29]
Hb-PIT@Fe_3O_4/GCE	0.1 M PBS pH = 7	0.002-0.35	0.54	–	[30]
Fe^{3+}/PB/H-PPy	0.5 M KCl HCl pH = 3.0	0.005-2.775	1.6	484.4	[31]
Fe-NGCs	0.1 M PB pH = 7	0.001-5	0.53z.star;	184.4	This work

z.star; Results are calculation by the same method.

the Fe-NGCs-modified GCEs among our prepared M-NGCs-modified GCEs. Thus, the sensory performances for H_2O_2 detection of the GCEs modified by Fe-NGCs are comparable even exceeded, compared with some of the precious metal-based sensors [1,3,5,7,11,12,19–21,24]. The main performance indicators of the GCE sensors modified by Fe-NGCs and other reported H_2O_2 sensors are listed in Table 1. Although some reported works achieved higher performance, the advantage of our work is that Fe-NGC can efficiently detect H_2O_2 without usage of noble metals or enzymes.

3.3. The selectivity and stability of the sensor

In real detection application, the selectivity is one of most important factors due to several substances such as glucose, ascorbic acid (AA) and uric acid (UA) dopamine (DA), Na_2SO_4, KOH are generally coexisting with H_2O_2 in real samples which may interfere original sensitivity to H_2O_2 detection [38–40]. Fig. 6a shows the amperometric response of Fe-NGNs electrode with sequentially adding 1 mM H_2O_2, 10 mM glucose, 10 mM AA, 10 mM UA, 10 mM DA, 10 mM Na_2SO_4, 10 mM KOH and 1 mM H_2O_2 at room atmosphere. The responsive current has significant changes after adding 1 mM H_2O_2. Even though the concentrations of glucose, AA, UA, DA, Na_2SO_4 and KOH are much larger than H_2O_2, there are small change of current. It is caused by adding additional 10 vol% PB solution to dissolve interfering substances to lead to a decrease in the concentration of H_2O_2. Thus, these kinds of potential interfering substances (such as glucose, AA, UA, DA, cations and anions) could not influence the modified GCEs for detection of H_2O_2, indicating the modified GCEs have high selectivity to the electrochemical detection of H_2O_2 in pH = 7 buffer solution. As Fe and N co-doped carbon materials are sharply developed to efficiently catalyst oxygen reduction, influence of O_2 concentration for detecting H_2O_2 with the GCEs modified by Fe-NGCs has been evaluated by testing the GCEs in N_2 or O_2 saturated 0.1 M PB solution. Results of detecting H_2O_2 have been compared in solution with degassing O_2 and in O_2 saturated one and no distinguished amperometric response has been found (Fig. 6b), indicating existence of O_2 can be ignored in detecting H_2O_2 by amperometry, when pH of the solution is around 7. Thus, Fe-NGCs-modified GCEs can detect H_2O_2 without degassing O_2, as major requirements of detecting H_2O_2 are carried out in the solution with pH of ~7. With alkalinity of the solution increasing, catalysis of Fe-NGCs towards O_2 reduction might rise, leading to such solution should be degassed before detection of H_2O_2. The stability of the modified GCEs is measured by CV and amperometry (Fig. S9). The retention rate of the responsive current is still 96.8 % after 100 tests cycles in 5 mM H_2O_2 solution (Fig. S9b), while the retention rate of the modified sensor is still 99 % (Fig. S9c: the sensor is tested in 5 mM H_2O_2 solution under

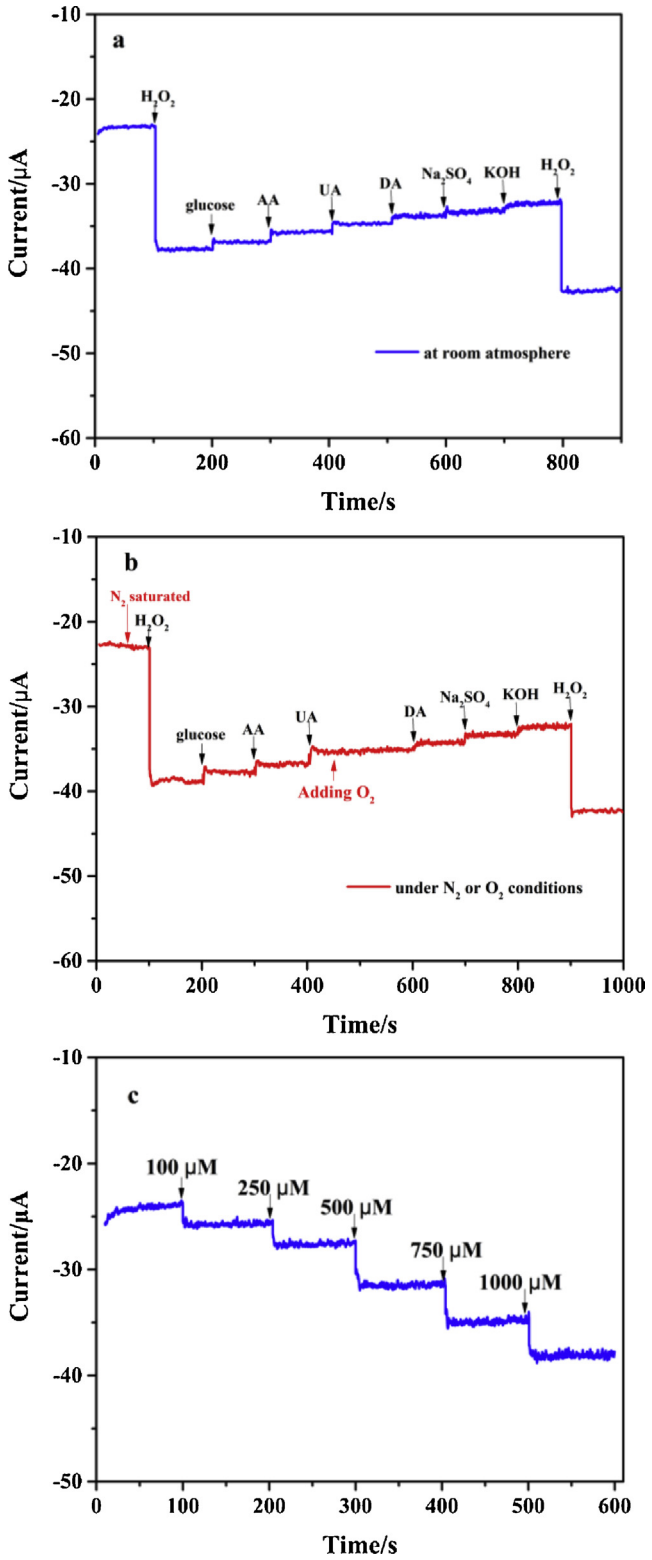

Fig. 6. Amperometric response of GCEs modified by Fe-NGCs to the additions of 1 mM H_2O_2, 10 mM glucose, 10 mM AA, 10 mM UA, 10 mM DA, 10 mM Na_2SO_4, 10 mM KOH and 1 mM H_2O_2 in 0.1 M phosphate buffer solution (a) or in N_2 saturated/O_2 saturated buffer solution (b). (c) i–t curve when detecting H_2O_2 in mixture of 20 vol% milk and 80 vol% PB buffer solution.

amperometric conditions after 1800s). Additionally, the response current of the Fe-NGC modified sensor after 50 CV cycles (Fig. S9d) is closed to that of the sensor without CV (Fig. 5a), indicating good stability of the Fe-NGC modified sensor.

3.4. Demonstration of practical applications

Hydrogen peroxide is used in the sterilization of the equipment for treating milk and fruit juice, while its presence can contaminate them. Detection of H_2O_2 in milk and fruit juice are investigated to further verify the feasibility of the GCEs modified by Fe-NGC in real sample [1,3,41]. Fig. 6c and Fig. S11a shows the amperometric response of the modified GCEs to H_2O_2 with adding H_2O_2. The corresponding polarization curve is shown in Fig. S10 and Fig. S11b, and the slope is calculated to be -13.72 (milk) and -13.42 (fruit juice), respectively. The recovery information in various concentrations of H_2O_2 is listed in Tab. S2. Compared with standard curve, the recovery rate of H_2O_2 is 103.0 % (milk) and 100.8 % (fruit juice), indicating the modified sensors could be applied in electrochemical detection of H_2O_2. H_2O_2 has also been detected in a lens cleaning liquid and a mouth wash liquid. With concentration of surfactant increasing, the performance of detecting H_2O_2 becomes poor in the solutions (Fig. S12, S13 and Tab. S2). As Fe-NGCs have a unique graphitic structure and high specific surface area, they might have other applications in wide areas as adsorbents, electrode materials, or energy storage media [42–50].

4. Conclusions

In summary, the nanocomposites based on N-doped porous-walled graphitic nanocages with high specific surface area have been successfully doped by transition metal ion (Fe, Co, Ni or Cu) towards efficient H_2O_2 electrochemical catalyst.

Fe-N coordination much easier forms in the condition of our experiment than Co-N, Ni-N and Cu-N, which might lead to excellent electrochemical performance of Fe-NGCs, including wider linear range ($0.001-5$ mM), lower LOD (0.53 μM), higher sensitivity ($184.4\ \mu A\ mM^{-1}\ cm^{-2}$), selectivity and stability. With high specific surface area ($920\ m^2\ g^{-1}$), mesopore volume ($1.6\ cm^3\ g^{-1}$) and good graphitization, the synergistic effects of Fe ions and N-doped structure, which improves dispersion of metallic ions and increases active sites, plays a very important role in detection of H_2O_2. In demonstration of practical applications, the Fe-NGCs is provided with good recovery rate. The results indicate that the prepared Fe-NGCs nanocomposite will be a potential material for the modification of noble-free metal H_2O_2 sensor.

Declaration of Competing Interest

The authors declare that they have no known competing financial interests or personal relationships that could have appeared to influence the work reported in this paper.

Acknowledgements

This research was supported by Pujiang Talent Project (13PJ1407400) and Funds (14520503100, 15520503400) from science and technology commission of Shanghai municipality, Funds from Shanghai institute of technology (ZQ2018-14, XTCX2017-1) and research fund (project #21306113) from the National Natural Science Foundation of China.

Appendix A. Supplementary data

Supplementary material related to this article can be found, in the online version, at doi:https://doi.org/10.1016/j.snb.2019.127550.

References

[1] M. Wang, J.W. Ma, X.L. Guan, W.C. Peng, X.B. Fan, G.L. Zhang, F.B. Zhang, Y. Li, A novel H_2O_2 electrochemical sensor based on $NiCo_2S_4$ functionalized reduced graphene oxide, J. Alloys. Compd. 784 (2019) 827–833, https://doi.org/10.1016/j.jallcom.2019.01.043.

[2] J. He, W. Zhou, J. Sunarso, X.M. Xu, Y.J. Zhong, Z.P. Shao, X.J. Chen, H. Zhu, 3D ordered macroporous $SmCoO_3$ perovskite for highly active and selective hydrogen peroxide detection, Electrochim. Acta 260 (2018) 372–383, https://doi.org/10.1016/j.electacta.2017.12.084.

[3] S.G. Leonardi, D. Aloisio, N. Donato, P.A. Russo, M.C. Ferro, N. Pinna, G. Neri, Amperometric sensing of H_2O_2 using Pt-TiO_2/Reduced graphene oxide nanocomposites, ChemElectroChem 1 (2014) 617–624, https://doi.org/10.1002/celc.201300106.

[4] H. Li, H.L. Zhao, H.Y. He, L.B. Shi, X. Cai, M.B. Lan, Pt-Pd bimetallic nanocoral modified carbon fiber microelectrode as a sensitive hydrogen peroxide sensor for cellular detection, Sens. Actuators B-Chem. 260 (2018) 174–182, https://doi.org/10.1016/j.snb.2017.12.179.

[5] H.J. Guan, Y. Liu, Z.J. Bai, J. Zhang, S.G. Yuan, B. Zhang, Ag nanoparticles embedded in N-doped carbon nanofibers: a superior electrocatalyst for hydrogen peroxide detection, Mater. Chem. Phys. 213 (2018) 335–342, https://doi.org/10.1016/j.matchemphys.2018.04.002.

[6] Y.P. Ye, T. Kong, X.F. Yu, Y.K. Wu, K. Zhang, X.P. Wang, Enhanced nonenzymatic hydrogen peroxide sensing with reduced graphene oxide/ferroferric oxide nanocomposites, Talanta 89 (2012) 417–421, https://doi.org/10.1016/j.talanta.2011.12.054.

[7] N.N. Lu, T.T. Zhang, X.Y. Yan, Y. Gu, H. Liu, Z.Q. Xu, H.X. Xu, X.W. Li, Z.Q. Zhang, M. Yang, Facile synthesis of 3D N-doped porous carbon nanosheets as highly active electrocatalyst toward the reduction of hydrogen peroxide, Nanoscale 10 (2018) 14923–14930, https://doi.org/10.1039/C8NR02573H.

[8] W. Liu, H.X. Zhang, B. Yang, Z.J. Li, L.C. Lei, X.W. Zhang, A non-enzymatic hydrogen peroxide sensor based on vertical NiO nanosheets supported on the graphite sheet, J. Electroanal. Chem. 749 (2015) 62–67, https://doi.org/10.1016/j.jelechem.2015.04.037.

[9] R. Zlatev, M. Stoytcheva, B. Valdez, Rapid reagent-less on-line H2O2 quantification in alkaline semiconductor etching solution, Part 2: Nephelometry application, Talanta 179 (2018) 594–600, https://doi.org/10.1016/j.talanta.2017.11.059.

[10] M.G. Ren, B.B. Deng, J.Y. Wang, X.Q. Kong, Z.R. Liu, K. Zhou, L.W. He, W.Y. Lin, A fast responsive two-photon fluorescent probe for imaging H_2O_2 in lysosomes with a large turn-on fluorescence signal, Biosens. Bioelectron. 79 (2016) 237–243, https://doi.org/10.1016/j.bios.2015.12.046.

[11] L. Zhao, K.A. Sun, N. Youliwasi, H.L. Guo, G. Yang, F. Jiao, B. Dong, Y.M. Chai, S. Mintova, C.G. Liu, Highly sensitive H_2O_2 sensor based on porous bimetallic oxide $Ce_{1-x}Tb_xO_y$ derived from homeotypic Ln-MOFs, Appl. Surf. Sci. 470 (2019) 91–98, https://doi.org/10.1016/j.apsusc.2018.10.278.

[12] X.X. Zhang, Y.Y. Bao, Y.F. Bai, Z.Z. Chen, J. Li, F. Feng, In situ electrochemical reduction assisted assembly of a graphene-gold nanoparticles@polyoxometalate nanocomposite film and its high response current for detection of hydrogen peroxide, Electrochim. Acta 300 (2019) 380–388, https://doi.org/10.1016/j.electacta.2019.01.084.

[13] H.C. Hu, H.J. Jin, X.S. Chai, Rapid determination of hydrogen peroxide in pulp bleaching effluents by headspace gas chromatography, J. Chromatogr. A 1235 (2012) 182–184, https://doi.org/10.1016/j.chroma.2012.02.069.

[14] D.L. Yu, P. Wang, Y.J. Zhao, A.P. Fan, Iodophenol blue-enhanced luminol chemiluminescence and its application to Hydrogen peroxide and glucose detection, Talanta 146 (2016) 655–661, https://doi.org/10.1016/j.talanta.2015.06.059.

[15] J.L. Zhu, W. Nie, Q. Wang, J.W. Li, H. Li, W. Wen, T. Bao, H.Y. Xiong, X.H. Zhang, S.F. Wang, In situ growth of copper oxide-graphite carbon nitride nanocomposites with peroxidase-mimicking activity for electrocatalytic and colorimetric detection of hydrogen peroxide, Carbon 129 (2018) 29–37, https://doi.org/10.1016/j.carbon.2017.11.096.

[16] R.Z. Zhang, S.J. He, C.M. Zhang, W. Chen, Three-dimensional Fe- and N-incorporated carbon structures as peroxidase mimics for fluorescence detection of hydrogen peroxide and glucose, J. Mater. Chem. B 3 (2015) 4146–4155, https://doi.org/10.1039/c5tb00413f.

[17] B. Xue, K.Z. Li, S.Y. Gu, L.L. Zhang, J.H. Lu, Ni foam-supported ZnO nanowires and Co_3O_4/$NiCo_2O_4$ double-shelled nanocages for efficient hydrogen peroxide detection, Sens. Actuators B-Chem. 262 (2018) 828–836, https://doi.org/10.1016/j.snb.2018.02.091.

[18] H.J. Guan, J. Zhang, Y. Liu, Y.F. Zhao, B. Zhang, Rapid quantitative determination of hydrogen peroxide using an electrochemical sensor based on PtNi alloy/CeO_2 plates embedded in N-doped carbon nanofibers, Electrochim. Acta 295 (2019) 997–1005, https://doi.org/10.1016/j.electacta.2018.11.126.

[19] J. Ju, W. Chen, In situ growth of surfactant-free gold nanoparticles on nitrogen-doped graphene quantum dots for electrochemical detection of Hydrogen Peroxide in Biological Environments, Anal. Chem. 873 (2015) 1903–1910, https://doi.org/10.1021/ac5041555.

[20] Z.Y. Yang, X.H. Zheng, J.B. Zhang, Non-enzymatic sensor based on a glassy carbon electrode modified with Ag nanoparticles/polyaniline/halloysite nanotube nanocomposites for hydrogen peroxide sensing, RSC Adv. 6 (2016) 58329–58336, https://doi.org/10.1039/c6ra06366g.

[21] A.K.M. Kafi, Q. Wali, R.J. Jose, T.K. Biswas, M.M. Yusoff, A glassy carbon electrode modified with SnO2 nanofibers, polyaniline and hemoglobin for improved amperometric sensing of hydrogen peroxide, Microchim. Acta 184 (2017) 4443–4450, https://doi.org/10.1007/s00604-017-2479-6.

[22] M. Baghayeri, H. Alinezhad, M. Tarahomi, M. Fayazi, M.G. Motlagh, B. Maleki, A non-enzymatic hydrogen peroxide sensor based on dendrimer functionalized magnetic graphene oxide decorated with palladium nanoparticles, Appl. Surf. Sci. 478 (2019) 87–93, https://doi.org/10.1016/j.apsusc.2019.01.201.

[23] R. Ramachandran, C. Zhao, M. Rajkumar, K. Rajavel, P. Zhu, W. Xuan, Z.-X. Xu, F. Wang, fPorous nickel oxide microsphere and Ti_3C_2Tx hybrid derived from metal-organic framework for battery-type supercapacitor electrode and non-enzymatic H_2O_2 sensor, Electrochim. Acta 322 (2019) 134771, , https://doi.org/10.1016/j.electacta.2019.134771.

[24] D.S. Achari, C. Santhosh, R. Deivasegamani, R. Nivetha, A. Bhatnagar, S.K. Jeong, A.N. Grace, A non-enzymatic sensor for hydrogen peroxide based on the use of α-Fe_2O_3 nanoparticles deposited on the surface of NiO nanosheets, Microchim. Acta 184 (2017) 3223–3229, https://doi.org/10.1007/s00604-017-2335-8.

[25] T. Balamurugan, V. Mani, C.C. Hsieh, S.T. Huang, T.K. Peng, H.Y. Lin, Real-time tracking and quantification of endogenous hydrogen peroxide production in living cells using graphenated carbon nanotubes supported Prussian blue cubes, Sens. Actuators B-Chem. 257 (2018) 220–227, https://doi.org/10.1016/j.snb.2017.10.151.

[26] H.J. Guan, Y.F. Zhao, J. Zhang, Y. Liu, S.G. Yuan, B. Zhang, Uniformly dispersed PtNi alloy nanoparticles in porous N-doped carbon nanofibers with high selectivity and stability for hydrogen peroxide detection, Sens. Actuators B-Chem. 261 (2018) 354–363, https://doi.org/10.1016/j.snb.2018.01.169.

[27] M. Guler, V. Turkoglu, A. Bulut, M. Zahmakiran, Electrochemical sensing of hydrogen peroxide using Pd@Ag bimetallic nanoparticles decorated functionalized reduced graphene oxide, Electrochim. Acta 263 (2018) 118–126, https://doi.org/10.1016/j.electacta.2018.01.048.

[28] R.Z. Zhang, W. Chen, Fe_3C-functionalized 3D nitrogen-doped carbon structures for electrochemical detection of hydrogen peroxide, Sci. Bull. 60 (2015) 522–531, https://doi.org/10.1007/s11434-015-0740-0.

[29] A.K. Dutta, S.K. Maji, D.N. Srivastava, A. Mondal, P. Biswas, P. Paul, B. Adhikary, Peroxidase-like activity and amperometric sensing of hydrogen peroxide by Fe_2O_3 and Prussian Blue-modified Fe_2O_3 nanoparticles, J. Molecular Catal. A Chem. 360 (2012) 71–77, https://doi.org/10.1016/j.molcata.2012.04.011.

[30] M. Baghayeri, M. Rouhi, M.M. Lakouraj, M.A. Aref, Bioelectrocatalysis of hydrogen peroxide based on immobilized hemoglobin onto glassy carbon electrode modified with magnetic poly(indole-co-thiophene) nanocomposite, J. Electroanal. Chem. 784 (2017) 69–76, https://doi.org/10.1016/j.jelechem.2016.12.006.

[31] Z. Yang, X. Zheng, J. Zheng, Facile synthesis of prussian Blue/Hollow polypyrrole nanocomposites for enhanced hydrogen peroxide sensing, Ind. Eng. Chem. Res. 55 (2016) 12161–12166, https://doi.org/10.1021/acs.iecr.6b02953.

[32] Z.M. Sheng, C.X. Guo, C.M. Li, Nitrogen-doping templated nanoporous graphitic nanocage and its supported catalyst towards efficient methanol oxidation, Electrochem. commun. 19 (2012) 77–80, https://doi.org/10.1016/j.electacta.2018.01.048.

[33] N.N. Li, Z.M. Sheng, H.L. Tian, C.K. Chang, R.P. Jia, S. Han, In situ approach of cementite nanoparticles encapsulated with nitrogen-doped graphitic shells as anode nanomaterials for Li-ion and Na-ion batteries, RSC Adv. 8 (2018) 33030–33034, https://doi.org/10.1039/c8ra05544k.

[34] Z.M. Sheng, X.J. Chang, Y.H. Chen, C.Y. Hong, N.N. Li, C.K. Chang, R.P. Jia, S. Han, Doping-template approach of porous-walled graphitic nanocages for superior performance anodes of lithium ion batteries, RSC Adv. 7 (2017) 42083–42087, https://doi.org/10.1039/c7ra07859e.

[35] Z.M. Sheng, M.H. Hu, X.Y. Dai, C.Y. Hong, C.C. Cheng, Q.Z. Chen, X.J. Chang, High-performance supercapacitor based on nanocages with nanoporous thin-walled graphitic shells, Microporous Mesoporous Mater. 234 (2016) 224–229, https://doi.org/10.1016/j.micromeso.2016.07.025.

[36] C.Y. Hong, Z.M. Sheng, M.H. Hu, X.Y. Dai, C.K. Chang, Q.Z. Chen, D.Y. Zhang, Thin-walled graphitic nanocages with nitrogen-doping as superior performance anodes for lithium-ion batteries, RSC Adv. 6 (2016) 59896–59899, https://doi.org/10.1039/C6RA10803B.

[37] K. Ozoemena, Z.X. Zhao, T. Nyokong, Immobilized cobalt(II) phthalocyanine–cobalt(II) porphyrin pentamer at a glassy carbon electrode: applications to efficient amperometric sensing of hydrogen peroxide in neutral and basic media, Electrochem. commun. 7 (2005) 679–684, https://doi.org/10.1016/j.elecom.2005.04.019.

[38] Z. Wang, F.Y. Xie, Z. Liu, G. Du, A. Asiri, X.P. Sun, High-performance non-enzyme hydrogen peroxide detection in neutral solution: using a nickel borate nanoarray as a 3D electrochemical sensor, Chem. Eur. J. 23 (2017) 16179–16183, https://doi.org/10.1002/chem.201704038.

[39] B.J. Hou, H.Z. Liu, S.P. Qi, Y.Y. Zhou, X.Q. Jiang, L.H. Zhu, Preparation of pristine graphene in ethanol assisted by organic salts for nonenzymatic detection of hydrogen peroxide, J. Colloid Interface Sci. 510 (2018) 103–110, https://doi.org/10.1016/j.jcis.2017.09.052.

[40] M.A. Riaz, S.L. Zhai, L. Wei, Z. Zhou, Z.W. Yuan, Y.Q. Wang, Q.W. Hang, X.Z. Liao, Y. Chen, Ultralow-platinum-loading nanocarbon hybrids for highly sensitive hydrogen peroxide detection, Sens. Actuators B-Chem. 283 (2019) 304–311, https://doi.org/10.1016/j.snb.2018.12.041.

[41] Z.M. Sheng, C.Y. Hong, N.N. Li, Q.Z. Chen, R.P. Jia, D.Y. Zhang, S. Han, Graphitic nanocages prepared with optimized nitrogen-doped structures by pyrolyzing selective precursors towards highly efficient oxygen reduction, Electrochim. Acta 259 (2018) 1104–1109, https://doi.org/10.1016/j.electacta.2017.12.080.

[42] N.N. Li, Z.M. Sheng, H. Huang, Z.Z. Gan, C.K. Chang, R.P. Jia, S. Han, Fe2O3 nanoparticles encapsulated with N-doped porous graphitic shells approached by oxidizing Fe_3C@C precursor for high-performance sodium-ion batteries, J. Alloys. Compd. 792 (2019) 25–31, https://doi.org/10.1016/j.jallcom.2019.04.008.

[43] L. Zhou, Y. Qiao, C.Y. Zhong, C.M. Li, Enabling fast electron transfer through both bacterial outer-membrane redox centers and endogenous electron mediators by polyaniline hybridized large-mesoporous carbon anode for high-performance microbial fuel cells, Electrochim. Acta 229 (2017) 31–38, https://doi.org/10.1016/j.electacta.2017.01.081.

[44] H. Jin, H. Guo, X. Gao, R. Gui, Selective and sensitive electrochemical sensing of gastrodin based on nickel foam modified with reduced graphene oxide/silver nanoparticles complex-encapsulated molecularly imprinted polymers, Sens. Actuators

B-Chem. 277 (2018) 14–21, https://doi.org/10.1016/j.snb.2018.08.156.
[45] B.M. Feng, X.J. Wu, Y.L. Niu, W. Li, Y.X. Yao, W.H. Hu, C.M. Li, Hierarchically porous Fe/N-C hollow spheres derived from melamine/Fe-incorporated polydopamine for efficient oxygen reduction reaction electrocatalysis, Sustain. Energy Fuels 3 (2019) 3455–3461 https://doi.org/101039/C9SE00686A.
[46] D.D. Sun, G.J. Liu, S.T. Liu, X.L. Jia, J.S. Zhou, A layered Bi_2Te_3 nanoplates/graphene composite with high gravimetric and volumetric performance for Na-ion storage, Sustain. Energy Fuels 3 (2019) 3163–3171, https://doi.org/10.1039/C9SE00544G.
[47] Z.Z. Gan, Z.M. Sheng, H. Huang, X.Y. Dai, R.L. Niu, R.P. Jia, Highly mesoporous Fe and N Co-doped graphitic catalysts prepared from short-time synthesis of precursor towards highly efficient oxygen reduction, Sustain. Energy Fuels 3 (2016) 3335–3343, https://doi.org/10.1039/C9E00532C.
[48] L. Bai, J.Q. Guan, Binary Ni2FeOx anchored on modified graphite for efficient and durable oxygen evolution electrocatalysis, Sustain. Energy Fuels 2 (2018) 2160–2164, https://doi.org/10.1039/C8SE00307F.
[49] G.V. Manohara, M.M. Valer, S. Garcia, A simple and green synthesis method for Ca-adamantanecarboxylate: a novel precursor for high temperature CO_2 capture sorbent materials, Sustain. Energy Fuels 3 (2019) 3318–3323, https://doi.org/10.1039/C9SE00451C.
[50] D.Q. Liu, Q.W. Li, J.B. Hou, H.Z. Zhao, Porous 3D graphene-based biochar materials with high areal sulfur loading for lithium–sulfur batteries, Sustain. Energy Fuels 2 (2018) 2197–2205, https://doi.org/10.1039/C8SE00343bB.

Zhao Min Sheng received his Bachelor and Ph. D. degree in materials science from Shanghai Jiao Tong university in 2003 and 2008. He fabricated novel carbon nanotubes and nanocages for fuel cell, superparamagnetism and supercapacitor applications. From 2009–2011, he worked as a postdoctoral research fellow in the school of chemical and biomedical engineering, Nanyang technology university, Singapore, for approaching novel carbon nanomaterials towards advanced biosensors. From 2019 to now, he works as an associate professor in SIT for synthesis of novel carbon nanomaterials for electrochemical applications.

Zu Zhong Gan received his Bachelor degree in materials science and engineering from Shanghai institute of technology (SIT) in 2017. He is investigating synthesis of novel carbonous nanomaterials for applications of biosensors and catalysts of oxygen reduction as a postgraduate student in SIT.

Huan Huang received his Bachelor degree in materials science and engineering from Gannan normal university in 2018. He is approaching novel graphitic nanomaterials by floating catalytic pyrolysis for electrode materials of Na/Li ion batteries and fuel cells as a postgraduate student in school of materials science and engineering, SIT.

Rui Liang Niu received his Bachelor degree in electronic encapsulation technology from Guilin university of electronic technology in 2018. He is approaching novel carbon-based nanomaterials for electrode materials of Na/Li ion batteries and supercapacitors as a postgraduate student in school of materials science and engineering, SIT.

Zhi Wei Han is a second-year undergraduate in school of materials science and engineering, SIT. He is studying for preparing and testing biosensors in a science innovation project of undergraduate student.

Run Ping Jia received her Ph. D. degree in in materials science from Lan Zhou university in 2004. She received an outstanding postdoctoral fellow reward from Tongji university in 2006. She is working as a full professor in SIT for synthesis of novel electrochemical, photoelectric and catalytic materials from polymers.